

Influence of niobium impurity on spin density in metallic iron

A. Błachowski¹, K. Ruebenbauer^{*, 1}, and J. Żukrowski²

¹ Mössbauer Spectroscopy Division, Institute of Physics, Pedagogical University,
ul. Podchorążych 2, 30 084 Kraków, Poland

² Solid State Physics Department, Faculty of Physics and Applied Computer Science,
AGH University of Science and Technology, Al. Mickiewicza 30, 30 059 Kraków, Poland

Received 18 May 2005, revised 7 September 2005, accepted 21 September 2005

Published online 3 November 2005

PACS 75.50.Bb, 76.80.+y

Random alloys of Nb in α -Fe with the Nb concentration up to about 5 at.% were investigated by means of Mössbauer spectroscopy at room temperature vs. Nb concentration. A solid solution saturates at about 2.3 at.% of Nb. Non-stoichiometric Fe₂Nb phase rich in Fe precipitates at higher Nb concentrations leaving α -Fe phase with about 1.6 at.% of Nb. The spin density of the iron atom is influenced in the α phase by the Nb atoms residing as nearest neighbours or second nearest neighbours. More distant impurities have no effect on the hyperfine parameters of Fe.

© 2005 WILEY-VCH Verlag GmbH & Co. KGaA, Weinheim

1 Introduction

Mössbauer spectroscopy is a good local probe of the charge and spin density on the nucleus of a resonant atom. Impurities dissolved randomly on the regular sites of the ferromagnetically ordered α -Fe phase have an effect on the density of the s-like electrons in their vicinity, and hence they influence the isomer shift and a transferred component of the hyperfine magnetic field as seen by the resonant Fe atom. It was found that major contributions to the above perturbations arise from the impurities located within three nearest neighbour coordination shells [1–5].

2 Experimental

Samples were prepared by arc melting under argon atmosphere of about 1.5 g of iron having 99.97 + at.% purity with the appropriate amount of niobium of 99.9 at.% purity. Samples were re-melted three times in order to assure homogeneity. The resulting Nb concentration was determined by means of an electron micro-probe. Samples containing more than about 2.3 at.% of Nb were characterised by islands of high Nb concentration characteristic of the formal Fe₂Nb phase rich in Fe. A solid solution saturated at about 2.3 at.% of Nb. Mössbauer spectra were collected at room temperature on powders embedded in epoxy resin discs. The powders were prepared with the help of a diamond file. The sample used to obtain the X-ray diffraction data was made using the same file. No structural changes were found due to the sample powdering by the above method. Additionally, an Al ingot was powdered with the help of the same diamond file and the Mössbauer spectrum of the resulting powder was collected for a prolonged time. No phases containing iron and originating from the material of the file were found. Absorbers contained about 30 mg/cm² of natural Fe and had 25-mm diameter. A contribution to the line width due to the sample thickness was about 5%, as the typical dimensionless absorber thickness was found to

* Corresponding author: e-mail: sfrueben@cyf-kr.edu.pl, Fax: +(48-12) 637-2243

be $t_a = 1.5$. A transmission integral algorithm was applied to all spectra (see the following section). A commercial $^{57}\text{Co}(\text{Rh})$ source maintained at room temperature was used to look for the 14.41 keV resonance. Spectra were collected in a round-corner triangular mirror mode with 4096 data channels per unfolded spectrum by means of a MsAa-3 spectrometer [6]. The sample having the highest Nb concentration was investigated additionally by means of the X-ray powder diffraction method.

3 Mössbauer data evaluation

The method of Mössbauer data treatment appropriate in the present case has been described in Ref. [1]. Here the formalism presented in Ref. [1] is repeated with some extensions to make the description complete.

The resonant absorption profile can be expressed in terms of sextets for the 14.41 keV transition from the ground to the first excited nuclear state of ^{57}Fe provided that the hyperfine interactions are time independent, and the non-scalar part of the hyperfine interactions is described entirely by the local effective magnetic field. Each of the above sextets can be written in the following form [7]:

$$L_{\{n_s, k_s\}}^{(\sigma)}(\omega) = \Gamma_a \sum_{\mu=1}^6 \left(\frac{b_\mu}{\Gamma_\mu} \right) \left\{ \frac{(\Gamma_\mu/2)^2}{(\Gamma_\mu/2)^2 + [\omega - \lambda_\mu^{(\sigma\{n_s, k_s\})}]^2} \right\}. \quad (1)$$

Here the symbol ω denotes the ambient energy of the absorbed radiation, usually expressed in velocity units of the applied Doppler motion between the source and the investigated absorber. The symbol Γ_a stands for the absorber half width without broadening, while the symbol Γ_μ can be expressed as $\Gamma_\mu = \sqrt{\Gamma_a^2 + \Delta\Gamma_\mu^2}$, where $\Delta\Gamma_\mu$ stands for the additional incoherent broadening due to the spurious hyperfine interactions and/or due to the incoming radiation beam divergence. Usually one can assume that the following relationship is valid: $\Delta\Gamma_1 = \Delta\Gamma_6$, $\Delta\Gamma_2 = \Delta\Gamma_5$ and $\Delta\Gamma_3 = \Delta\Gamma_4 = 0$. The above corrections to the half widths are the same for all sextets. Relative intensities of the particular lines within the sextet can be calculated as follows provided that the temperature is high enough to equalise the populations of the all ground-state nuclear hyperfine levels:

$$b_1 = b_6 = \frac{3G}{4(1+2G)}, \quad b_2 = b_5 = \frac{1}{2(1+2G)}, \quad b_3 = b_4 = \frac{G}{4(1+2G)}. \quad (2)$$

The parameter $G \geq \frac{1}{2}$ stands for the diagonal element of the reduced dipolar anisotropy tensor and it accounts for the eventual anisotropy of the absorber, the latter anisotropy being mainly caused by the residual magnetisation of the sample [8]. For completely random samples exhibiting an isotropic recoilless fraction the following condition is satisfied: $G = 1$. Usually one can assume that the residual magnetisation has no effect on the hyperfine magnetic fields, and that it is the same for all sextets involved. Positions of the particular lines within the sextet can be calculated according to the following expressions [7]:

$$\begin{aligned} \lambda_1^{(\sigma\{n_s, k_s\})} &= -\frac{3}{2}\alpha_e^{(\sigma\{n_s, k_s\})} - \frac{1}{2}\alpha_g^{(\sigma\{n_s, k_s\})} + S_\sigma(\{n_s, k_s\}), \\ \lambda_2^{(\sigma\{n_s, k_s\})} &= -\frac{1}{2}\alpha_e^{(\sigma\{n_s, k_s\})} - \frac{1}{2}\alpha_g^{(\sigma\{n_s, k_s\})} + S_\sigma(\{n_s, k_s\}), \\ \lambda_3^{(\sigma\{n_s, k_s\})} &= +\frac{1}{2}\alpha_e^{(\sigma\{n_s, k_s\})} - \frac{1}{2}\alpha_g^{(\sigma\{n_s, k_s\})} + S_\sigma(\{n_s, k_s\}), \\ \lambda_4^{(\sigma\{n_s, k_s\})} &= -\frac{1}{2}\alpha_e^{(\sigma\{n_s, k_s\})} + \frac{1}{2}\alpha_g^{(\sigma\{n_s, k_s\})} + S_\sigma(\{n_s, k_s\}), \\ \lambda_5^{(\sigma\{n_s, k_s\})} &= +\frac{1}{2}\alpha_e^{(\sigma\{n_s, k_s\})} + \frac{1}{2}\alpha_g^{(\sigma\{n_s, k_s\})} + S_\sigma(\{n_s, k_s\}), \\ \lambda_6^{(\sigma\{n_s, k_s\})} &= +\frac{3}{2}\alpha_e^{(\sigma\{n_s, k_s\})} + \frac{1}{2}\alpha_g^{(\sigma\{n_s, k_s\})} + S_\sigma(\{n_s, k_s\}). \end{aligned} \quad (3)$$

The magnetic coupling constant in the excited nuclear state takes the following form: $\alpha_e^{(\sigma\{n_s, k_s\})} = \mu_N |g_e| B_\sigma(\{n_s, k_s\}) / \hbar q_0$, while the corresponding coupling constant in the ground nuclear state is

expressed as $\alpha_g^{(\sigma \{n_s, k_s\})} = \mu_N |g_g| B_\sigma(\{n_s, k_s\}) / \hbar q_0$ [7]. Here the symbol μ_N stands for the nuclear magneton, g_e stands for the nuclear gyro-magnetic factor in the excited nuclear state, while the symbol g_g denotes the corresponding gyro-magnetic factor in the ground nuclear state. The symbol \hbar denotes Planck's constant divided by 2π , while the symbol q_0 stands for the wave number of the absorbed radiation – at resonance. The latter parameter may be treated as constant due to the narrowness of the Mössbauer spectrum – on the energy scale of the resonant γ -ray. The Bohr–Weisskopf hyperfine anomaly may be neglected for the nuclear transition considered here. The parameter $S_\sigma(\{n_s, k_s\})$ stands for the total shift of the particular sextet relative to the unpolarised single-line source used. The source is usually thin as far as the resonant self-absorption is concerned. This shift is due to the isomer shift and eventual second-order Doppler shift.

The resonant absorption profile due to the phase exhibiting the above sextets may be calculated according to the following expression [1]:

$$L_0(\omega) = \sum_{s=1}^{\sigma} \sum_{k_s=0}^{n_s} C_\sigma(c | \{n_s, k_s\}) L_{\{n_s, k_s\}}^{(\sigma)}(\omega). \quad (4)$$

It is assumed that the recoilless fraction is isotropic and the same for all configurations leading to various sextets. If the additional non-magnetic phase containing iron is present, one can define an additional absorption profile in the following form:

$$L_D(\omega) = \Gamma_a \sum_{l=1}^L \left(\frac{b_l}{\Gamma_l} \right) \left\{ \frac{(\Gamma_l/2)^2}{(\Gamma_l/2)^2 + (\omega - \lambda_l)^2} \right\} \quad \text{with} \quad \sum_{l=1}^L b_l = 1. \quad (5)$$

Here the symbol b_l denotes the relative contribution due to the particular l -th line of the additional phase, Γ_l stands for the half width of this line, while the parameter λ_l describes the position of this line – on the same scale as the line positions of the main phase. The index L stands for the number of lines due to the additional phase (or phases). The total absorption profile takes the following form:

$$L(\omega) = (1 - b_D) L_0(\omega) + b_D L_D(\omega). \quad (6)$$

The parameter b_D describes the relative contribution due to the presence of the resonant atoms in the additional phase provided that the recoilless fractions are the same in both phases.

The spectrum shape may be calculated in a straightforward manner in the transmission integral approximation, and the respective expression describing the spectrum shape takes the following form [9]:

$$P(\nu) = A_0 \left\{ 1 - \left(\frac{f_s}{\lambda} \right) + \left(\frac{\Gamma_s f_s}{2\pi\lambda} \right) \int_{-\infty}^{+\infty} d\omega \left(\frac{1}{(\Gamma_s/2)^2 + (\omega - \nu)^2} \right) \exp[-t_a L(\omega)] \right\}. \quad (7)$$

Here the symbol ν stands for the relative velocity between the source and the absorber – along the beam, A_0 denotes the number of counts per data channel far off the resonance, while the symbol f_s stands for the source recoilless fraction along the emitted beam. The symbol Γ_s denotes the half width of the source, while the symbol t_a stands for the dimensionless absorber thickness for the resonant absorption. The parameter $\lambda \geq 1$ accounts for the non-resonant photons accepted by the detector within the single channel analyser window. It has to be noted that the dimensionless absorber thickness follows from the relationship $t_a = \rho \sigma_0 f_a (\Gamma/\Gamma_a) d$. Here the symbol ρ stands for the average density of the resonant nuclei within the absorber, σ_0 denotes the cross section for resonant absorption, f_a stands for the recoilless fraction of the absorber, Γ denotes the natural half width and d stands for the absorber thickness along the beam.

Different sextets are due to the various impurity configurations around the resonant atom. In the case of the BCC α -Fe substituted randomly by some impurity on the regular lattice sites, one can use the approximation described below provided that the impurity concentration c satisfies the following condition: $c \ll 1$. Namely, the intensities of particular sextets follow from the binomial distribution and they

take the following form [1]:

$$C_{\sigma}(c | \{n_s k_s\}) = \prod_{s=1}^{\sigma} \left[\left(\frac{n_s!}{(n_s - k_s)! k_s!} \right) c^{k_s} (1-c)^{n_s - k_s} \right]. \quad (8)$$

Here the index $s = 1, 2, \dots, \sigma$ enumerates subsequent coordination shells around the resonant atom until the outermost shell is taken into account, the latter shell being described by the index s taking the value σ . The index n_s stands for the number of vortices in the s -th shell, while the index $k_s = 0, 1, \dots, n_s$ stands for the number of impurities in the s -th shell. It is assumed that the impurities act in an additive way, and that a particular configuration within the shell has no effect on the hyperfine interactions. The weights described by the expression (8) are normalised, i.e. the following relationship is satisfied [1]:

$$\sum_{s=1}^{\sigma} \sum_{k_s=0}^{n_s} C_{\sigma}(c | \{n_s k_s\}) = 1. \quad (9)$$

The set of indices $\{n_s k_s\}$ represents a particular sextet for a definite value of the index σ . The corresponding hyperfine magnetic fields and shifts, the latter being dominated by the isomer shifts, are described by the following expressions, respectively [1]:

$$B_{\sigma}(\{n_s k_s\}) = B_0^{(\sigma)} + \sum_{s=1}^{\sigma} k_s \Delta B_s \quad \text{and} \quad S_{\sigma}(\{n_s k_s\}) = S_0^{(\sigma)} + \sum_{s=1}^{\sigma} k_s \Delta S_s. \quad (10)$$

Here the symbol $B_0^{(\sigma)}$ denotes the hyperfine field experienced by the resonant iron atom surrounded by pure iron until the outermost shell inclusive, while the symbol ΔB_s denotes a contribution to the hyperfine field due to a single impurity located in the s -th shell. It is assumed that all contributions to the hyperfine field are parallel or anti-parallel to the same local direction. Similarly, the symbol $S_0^{(\sigma)}$ stands for the total shift experienced by the iron atom surrounded by pure iron until the outermost shell inclusive, while ΔS_s denotes a contribution to the shift caused by a single impurity located in the s -th shell. The last contribution is practically due to the change in the isomer shift. The average hyperfine field and the average shift may be expressed as follows, respectively [1]:

$$\begin{aligned} \langle B \rangle_{\sigma} &= \sum_{s=1}^{\sigma} \sum_{k_s=0}^{n_s} C_{\sigma}(c | \{n_s k_s\}) B_{\sigma}(\{n_s k_s\}) = B_0^{(\sigma)} + c \sum_{s=1}^{\sigma} n_s \Delta B_s, \\ \langle S \rangle_{\sigma} &= \sum_{s=1}^{\sigma} \sum_{k_s=0}^{n_s} C_{\sigma}(c | \{n_s k_s\}) S_{\sigma}(\{n_s k_s\}) = S_0^{(\sigma)} + c \sum_{s=1}^{\sigma} n_s \Delta S_s. \end{aligned} \quad (11)$$

The model outlined above depends on a relatively small number of the adjustable parameters. Therefore, one can use it in order to fit the experimental data in the standard iterative way. Here the $\sigma = 2$ model was used, i.e. the first two coordination shells were taken into account. The indices n_1 and n_2 take the following values for the BCC structure: $n_1 = 8$ and $n_2 = 6$.

4 Discussion of results

Mössbauer data were evaluated by applying the *Gmbern* programme of the MOSGRAF data-evaluation system [10] in accordance with the formalism described in the previous section and in Ref. [1]. Results obtained within the solubility limit are summarised in Table 1, while the corresponding spectra are shown in Fig. 1. The $\sigma = 2$ model was used [1] as stated above, i.e. individual impurities up to the second coordination shell inclusive were considered. It was found that Nb has no effect on the total shift in the solute phase within our experimental accuracy. Here the total shift is primarily due to the isomer shift at least for the α -Fe phase with some dissolved niobium. All shifts are reported here vs. pure α -Fe, the latter maintained at room temperature. Hence, one can conclude that the electron charge density on the

Table 1 Hyperfine parameters seen on the iron nucleus in the pure α -phase are shown vs. niobium concentration. The last row shows respective averages, if applicable. The ϵ -phase is absent for these samples.

c [at.%]	$\langle B \rangle_2$ [T]	$B_0^{(2)}$ [T]	ΔB_1 [T]	ΔB_2 [T]	$\langle S \rangle_2$ [mm/s]	$S_0^{(2)}$ [mm/s]	ΔS_1 [mm/s]	ΔS_2 [mm/s]
	± 0.02	± 0.02			± 0.002	± 0.002		
0	32.97				0			
0.73	32.73	33.01	-3.55	-2.31	0	0.002	-0.03	-0.01
± 0.03			± 0.35	± 0.50			± 0.04	± 0.05
0.90	32.67	32.99	-3.54	-2.37	-0.001	0.002	-0.04	-0.02
± 0.05			± 0.41	± 0.68			± 0.04	± 0.06
1.66	32.43	33.06	-3.57	-2.32	0.001	0.005	-0.03	-0.01
± 0.07			± 0.16	± 0.24			± 0.02	± 0.02
2.30	31.99	33.04	-3.54	-2.19	-0.002	0.005	-0.03	-0.02
± 0.07			± 0.22	± 0.35			± 0.02	± 0.03
			-3.55	-2.30				
			± 0.15	± 0.24				

iron nucleus remains unperturbed in comparison with pure iron. On the other hand, the nearest-neighbour Nb atom decreases the iron hyperfine field by $\Delta B_1 = -3.55$ T, while the second nearest neighbour acts similarly albeit less effectively as the change is $\Delta B_2 = -2.30$ T. The average hyperfine field $\langle B \rangle_2$ and the field due to outer shells beyond the second shell $B_0^{(2)}$ are shown in Fig. 2 vs. Nb concentration c . More distant Nb atoms have no effect on the spin density of the iron nucleus, as the parameter $B_0^{(2)}$ remains practically constant vs. concentration.

Results for the mixed phase region (α -Fe with solute Nb and precipitated non-stoichiometric ϵ -Fe₂Nb [11]) are summarised in Table 2, while the spectra are shown in Fig. 1. The ϵ -phase remains paramag-

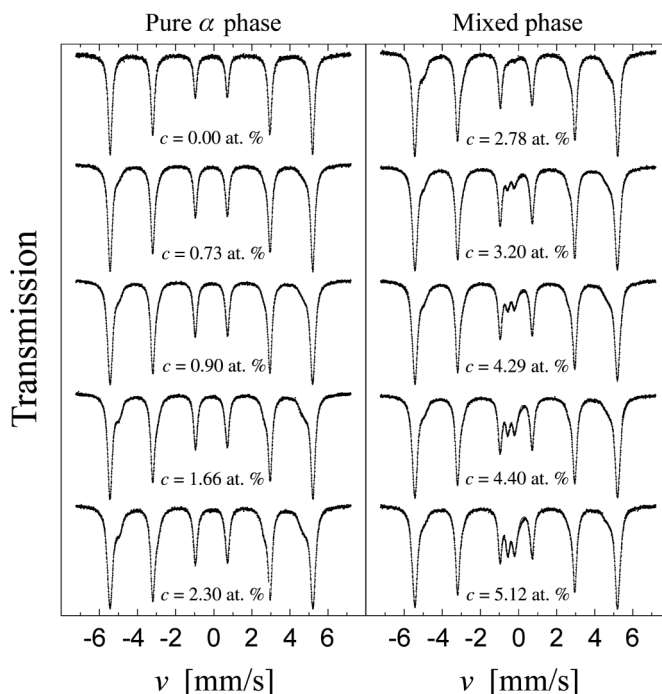
**Fig. 1** Mössbauer spectra are shown vs. niobium concentration.

Table 2 Hyperfine parameters obtained in the mixed phase region. The symbol C_{Nb} stands for the overall concentration of niobium. The symbol C_{M} denotes the contribution to the Mössbauer spectrum due to the ϵ -phase, S denotes the total shift of the spectrum due to this phase, while the parameter ΔE denotes the quadrupole splitting.

α -Fe(Nb)									
C_{Nb} [at.%]	c [at.%]	$\langle B \rangle_2$ [T] ± 0.02	$B_0^{(2)}$ [T] ± 0.02	ΔB_1 [T]	ΔB_2 [T]	$\langle S \rangle_2$ [mm/s] ± 0.002	$S_0^{(2)}$ [mm/s] ± 0.002	ΔS_1 [mm/s]	ΔS_2 [mm/s]
2.78	2.18	32.47	33.05	-3.68 ± 0.19	-2.36 ± 0.29	0.002	0.006	-0.03 ± 0.02	-0.01 ± 0.03
3.20	1.82	32.61	32.98	-3.62 ± 0.37	-2.39 ± 0.61	-0.001	0.003	-0.04 ± 0.04	-0.02 ± 0.06
4.29	2.26	32.54	32.97	-3.73 ± 0.34	-2.42 ± 0.56	-0.003	0.002	-0.04 ± 0.04	-0.03 ± 0.06
4.40	1.57	32.63	33.00	-3.72 ± 0.43	-2.60 ± 0.72	0.001	0.003	-0.03 ± 0.05	0 ± 0.05
5.12	1.44	32.63	33.00	-3.80 ± 0.84	-2.43 ± 0.93	0.004	0.002	-0.06 ± 0.05	-0.05 ± 0.10

ϵ -Fe ₂ Nb				
C_{Nb} [at.%]	c [at.%]	S [mm/s]	ΔE [mm/s]	C_{M} [%]
2.78	18.95	-0.21 ± 0.17	0.37 ± 0.30	2.4 ± 0.8
3.20	21.21	-0.24 ± 0.03	0.36 ± 0.06	5.5 ± 0.3
4.29	21.61	-0.24 ± 0.03	0.37 ± 0.04	8.1 ± 0.2
4.40	20.41	-0.24 ± 0.02	0.38 ± 0.02	11.3 ± 0.1
5.12	18.17	-0.24 ± 0.01	0.37 ± 0.02	14.7 ± 0.1

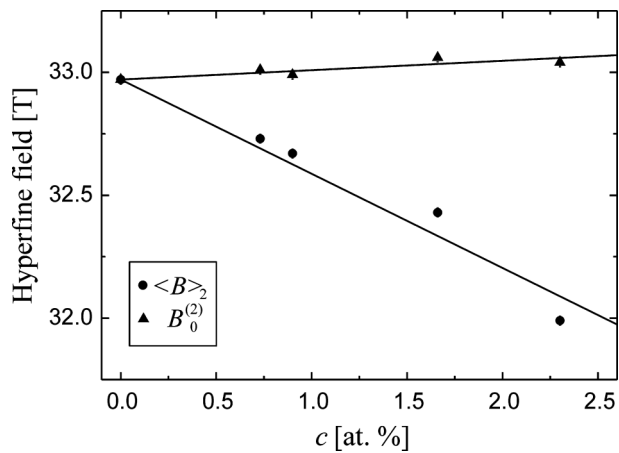


Fig. 2 Hyperfine fields are plotted vs. niobium concentration in the α -phase.

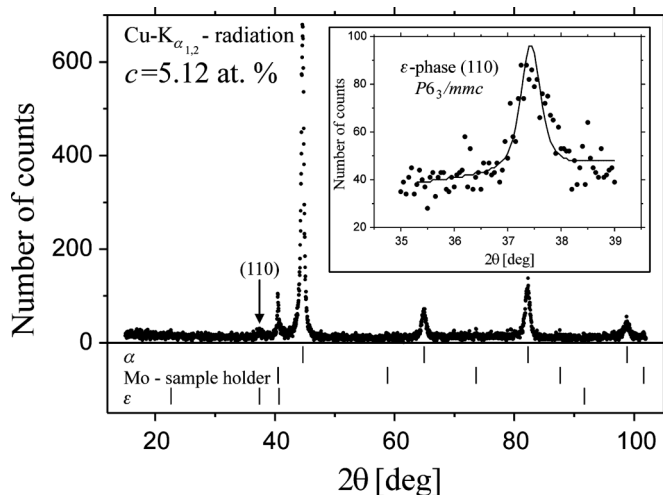


Fig. 3 Powder X-ray diffraction pattern of the sample having the highest overall niobium concentration is shown vs. scattering angle 2θ . The inset shows the pattern obtained for a prolonged counting time in the vicinity of the strongest reflection of the ϵ -phase. Vertical bars indicate maxima of the strongest possible Bragg reflections.

netic at room temperature, and it is characterised by the symmetric electric quadrupole-split doublet [12]. Hyperfine parameters of this phase do not depend on the original Nb concentration. Other investigators obtained similar spectra for the ϵ -phase in the vicinity of room temperature [12, 13]. It appears that the ϵ -phase is formed here far from stoichiometry, and it is richer in iron than follows from the chemical formula. It contains here about 20 at.% of Nb calculated as the average over respective samples with various concentrations of Nb. These results were obtained by means of the electron micro-probe. They are consistent with the observed contributions of the ϵ -phase to the Mössbauer spectra under the natural assumption that recoilless fractions are comparable in both phases. The α -phase reaches saturation of the Nb concentration at about 2.3 at.%. More concentrated samples decompose into two phases. It is interesting to note that the matrix α is depleted in Nb as compared with the saturation concentration (see Table 2). Hence, it may be concluded that Nb tends to transfer to the ϵ -phase from the α -phase.

The sample having the highest overall niobium concentration 5.12 at% has been investigated by means of the powder X-ray diffraction method at room temperature. Results are shown in Fig. 3. The hexagonal Laves ϵ -Fe₂Nb phase having the group symmetry $P6_3/mmc$ has been found [11] in addition to the α -Fe BCC phase with some dissolved niobium. The lattice constant of the α -phase was found as 0.28727(4) nm, in contrast to the pure α -Fe lattice constant being 0.28665 nm [11]. Lattice parameters of the ϵ -phase were found as $a = 0.4818(2)$ nm and $c = 0.7870(6)$ nm, while the same phase having a composition close to stoichiometry has the lattice constants $a_0 = 0.4821$ nm and $c_0 = 0.7877$ nm [14]. It is obvious that all lattice constants expand with the addition of niobium, as niobium atoms are larger than iron atoms. Therefore, the X-ray diffraction data confirm the previous statement that the ϵ -phase found here is rich in iron, i.e. some Nb sites are occupied by iron – probably at random.

The niobium impurity has a similar effect on the spin density seen by the iron nucleus in the α -phase as the osmium impurity [5]. Both these atoms decrease the spin density of iron. The second Nb neighbour has a stronger influence than the second Os neighbour, but more distant Nb impurities have practically no effect on the above spin density (see Fig. 2), in contrast to the Os atoms, the latter causing a weak increase of the spin density on iron.

Acknowledgements Dr. Janusz Przewoźnik, Solid State Physics Department, Faculty of Physics and Applied Computer Science, AGH University of Science and Technology, Kraków, Poland is warmly thanked for performing a powder X-ray diffraction investigation of one of the samples.

References

- [1] A. Błachowski, K. Ruebenbauer, and J. Żukrowski, *Phys. Scr.* **70**, 368 (2004).
- [2] T. Zemčik, in: *Proc. Int. Conf. Mössbauer Spectroscopy*, Vol. 2, edited by A. Z. Hryniewicz and J. A. Sawicki (Akademia Górniczo-Hutnicza Cracow, 1975), pp. 59–81.
- [3] J. Korecki and U. Gradmann, *Phys. Rev. Lett.* **55**, 2491 (1985).
- [4] J. Cieślak and S. M. Dubiel, *J. Alloys Compd.* **350**, 17 (2003).
- [5] A. Błachowski, K. Ruebenbauer, and J. Żukrowski, *Nukleonika* **49**, S67 (2004).
- [6] R. Górnicki, *RENON* [<http://www.renon.strefa.pl>].
- [7] N. N. Greenwood and T. C. Gibb, *Mössbauer Spectroscopy* (Chapman and Hall, London, 1971).
- [8] K. Ruebenbauer, *Physica B* **172**, 346 (1991).
- [9] S. Margulies, P. D. Debrunner, and H. Frauenfelder, *Nucl. Instrum. Methods* **21**, 217 (1963).
- [10] K. Ruebenbauer and T. Birchall, *Hyperfine Interact.* **7**, 125 (1979) [<http://www.elektron.ap.krakow.pl>].
- [11] T. B. Massalski, *Binary Alloy Phase Diagrams*, Vol. 1, 2nd edn. (ASM International, Materials Park, Ohio, USA, 1990).
- [12] M. T. Raposo, J. D. Ardisson, A. I. C. Persiano, and R. A. Mansur, *Hyperfine Interact.* **83**, 235 (1994).
- [13] S. Gupta, K. B. Lal, T. M. Srinivasan, and G. N. Rao, *phys. stat. sol. (a)* **22**, 707 (1974).
- [14] Powder Diffraction File, File No. PDF #150316 (The International Centre for Diffraction Data, Newton Square, Pennsylvania, USA, 1999).